

Article

A Novel Inductor for Stabilizing the DC Link of Adjustable Speed Drive

Qian Wang¹, Bingyang Luo^{2,*}, Jun Wang³, Zhe Kong² and Feng Liu²¹ Department of Energy, Aalborg University, 9220 Aalborg, Denmark; qiw@et.aau.dk² School of Automation, Wuhan University of Technology, Wuhan 430000, China; kz@whut.edu.cn (Z.K.); whutliufeng@163.com (F.L.)³ Wuhan Branch of China Classification Society (CCS), Wuhan 430000, China; wangjun@ccs.org.cn

* Correspondence: luobingy@whut.edu.cn

Abstract: The DC-link filter which includes a magnetic inductor and a storage capacitor is one of the key parts of adjustable speed drives in the market. It significantly affects the stability, reliability, and power density of the motor-drive system. This paper proposes a novel, variable active inductor to improve the performance of DC links in terms of stability, reliability, size, and cost. In contrast to conventional DC-link magnetic inductors, the variable active inductor is made of power electronic circuits, including active switches, passive filters, and smart controllers, which no longer rely on magnetic material. The demonstration shows that the inductor can emulate the electrical characteristics of the magnetic inductor for filtering harmonics and stabilizing the DC link, meanwhile representing a smaller size, lighter weight, and lower cost compared with a conventional one. Furthermore, this paper proposes a variable inductance control method which is able to adaptively tune the inductance value with the operating conditions of the drive system. The DC link can be stabilized, and high performance can be maintained in both balanced and unbalanced grid voltage conditions. A case study of the proposed variable inductor in a motor drive with a three-phase diode-bridge rectifier as the front end is discussed. Experimental results are given to verify the functionality and effectiveness of the proposed variable inductor.

Keywords: DC-link inductor; adjustable speed drive; magnetic inductor; unbalanced grid voltage



Citation: Wang, Q.; Luo, B.; Wang, J.; Kong, Z.; Liu, F. A Novel Inductor for Stabilizing the DC Link of Adjustable Speed Drive. *Electronics* **2021**, *10*, 2401. <https://doi.org/10.3390/electronics10192401>

Academic Editor: M. Tariq Iqbal

Received: 20 September 2021

Accepted: 28 September 2021

Published: 1 October 2021

Publisher's Note: MDPI stays neutral with regard to jurisdictional claims in published maps and institutional affiliations.



Copyright: © 2021 by the authors. Licensee MDPI, Basel, Switzerland. This article is an open access article distributed under the terms and conditions of the Creative Commons Attribution (CC BY) license (<https://creativecommons.org/licenses/by/4.0/>).

1. Introduction

The advancement of power electronic devices and their decreasing price due to market demands has increased the use of grid-connected Adjustable Speed Drive (ASD) systems as an effective energy saving solution in various industrial, commercial and residential applications [1,2]. DC-link filters are an important part of a standard ASD, in terms of stability, reliability, size, weight, and cost. It serves to limit the DC-link voltage ripple, absorb harmonics, and provide certain amount of energy storage for abnormal and transient operations [3,4].

In the standard ASD system, a DC-link filter including a large magnetic inductor and electrolytic capacitor is preferred due to cost effectiveness and simplicity. The criteria for sizing DC links come mostly from the stability and power-quality point of view, such as voltage and current ripple limitations, dynamic response, hold-up energy requirement, stability of the overall grid-connected drives, and so on [5]. These DC links work well for now, however, they also raise challenges on performance improvement in the next generation of products from following aspects:

- The DC-link inductor is commonly selected based on stability, power quality, and reliability criteria. It is always large and cannot be reduced, due to the functionality requirements for grid-current sharpening and DC-link ripple mitigation [6,7]. The use of these large-value magnetic inductors raises concerns about their size, weight, and cost. They are made of a magnetic core and copper coil, which are large and

heavy. Since their invention in the 1800s, research has continued. By developing new core material and optimizing the inductor structure, their performance improves approximately 10% per decade in terms of power density and efficiency. This is good progress but compared to the 500% improvement per decade of power semiconductors in power electronic systems, their inferior position becomes more obvious. Until now, the inductor has taken up around 20–40% of the volume and weight and has been identified as the bottleneck of the whole system [8]. Therefore, a high-density inductor to replace the existing magnetic inductor is expected.

- The use of a large inductor and electrolytic capacitor raises concerns on the stability and reliability of the DC links [9]. In a normal operation with the three-phase balanced grid condition, the DC-link capacitor and inductor can filter out six times the fundamental frequency harmonics at the DC link and stabilize the DC voltage. However, when the grid voltage is unbalanced, there will be two-times the fundamental frequency harmonics at the DC link, which is further amplified by the resonant magnetic inductor and storage capacitor [10–13]. This oscillation is unexpected and leads to an unstable DC-link voltage and the failure of electrolytic capacitors and inverter stage [9]. Therefore, methods to stabilize the DC-link voltage and mitigate the DC-link oscillation in both the balanced and unbalanced grid voltage conditions are demanded practically.

In order to cope with these practical challenges, both industrial and academic researchers have made considerable efforts, which are discussed below:

- The first category of methods is the use of a slim drive with only a film capacitor at the DC link, which is proposed to reduce the size, weight, and cost, and improve the reliability of the ASD [1,2]. However, the DC-link voltage has a large oscillation, which leads to challenges in the control and modulation of the inverter stage and higher electrothermal stress on the switching devices of the inverter.
- The second category of methods is to use an advanced active capacitor to replace the existing DC-link capacitor [14–16]. The active capacitor is made of a power electronic circuit and can emulate the electrical characteristics of the large electrolytic capacitor to stabilize the DC-link voltage. However, the active capacitor is parallel at the DC link and it has no contribution to the magnetic inductor reduction due to the large inductance needed for sharpening the grid current.
- The last category of methods is to design an active inductor to replace the magnetic inductor [17–19]. Similarly to the active capacitor, by using the power electronic circuits in the active inductor it is able to reduce size and weight. Because the inductor is connected in series with the DC link, it has the possibility to sharpen the grid current and stabilize the DC link at the same time. The concept of the fixed active inductor has been proposed and demonstrated before. It proves only the concept, and still has limitations that need to be studied more practically. Specifically, for the DC link of motor drives, the research challenges are:
 - It is still not clear what the quantitative benefits of the active inductor are compared to the passive inductors in specific applications and in terms of volume, weight, and cost, which are concerns in the industry.
 - Existing research has emulated a fixed inductor to prove the concept, the adaptive variable inductor has never been proposed before. For real applications, considering the grid voltage and unbalanced grid conditions, how to have the variable inductor adaptively change with the operating conditions to satisfy the grid code and DC-link stability and reliability requirements is still an open question.

This paper proposes a novel variable active inductor for the DC link of an ASD system. The contributions are:

- (1) Study the reliability-oriented design of the variable inductor. The quantitative benefits of the variable inductor in terms of size, weight, and cost can be identified.

- (2) Propose a variable control method to stabilize the DC link at both unbalanced and balanced grid voltage conditions.

Prototypes are manufactured to verify the accuracy of the modeling results and functionality of the adaptive variable inductance control for different grid conditions.

2. Overview of the Adjustable Speed Drive with DC-Link Inductor

The structure of the adjustable speed drive with the DC-link magnetic inductor and active inductor are presented in this section [1]. Figure 1 shows the block diagram of the three-phase grid-connected ASD with the specification in Table 1 investigated in this paper. It shows the conventional drive, which is implemented with a DC-link LC filter [20]. A large size DC-link magnetic inductor is used to reduce the line current harmonics as well as a large DC capacitor to limit the DC-link voltage fluctuation. The DC-link capacitor is implemented with two electrolytic capacitors connected in series for higher voltage rating, and then two in parallel for large capacitance. The magnetic inductor is selected based on the requirements of the grid code and DC-link ripple limitation, which is bulky and heavy.

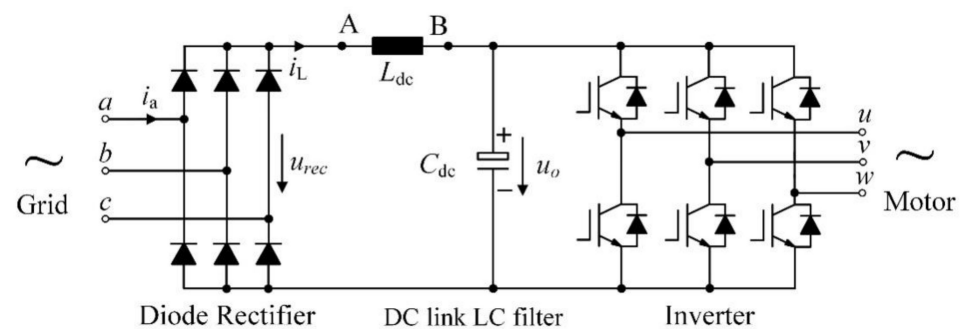


Figure 1. System structure of the adjustable speed drive (ASD) system with the DC-link LC filter. L_{dc} is the DC-link magnetic inductor, which would be replaced by the variable active inductor.

Table 1. Specification of an ASD system for performance comparison.

	Parameters	Description	Value
Three-phase diode-bridge rectifier	P	Power rating	7.5 kW
	V_s	AC voltage (RMS)	220 V
	f_s	Fundamental frequency	50 Hz
DC-link capacitor	C_{dc}	DC capacitor C_{dc}	680 μ F
Passive inductor	L	Passive inductor L	2.5 mH
Active inductor	L_{filter}	Filter inductor L_{filter}	250 μ H
	C_{dc}	DC-side C_{dc}	820 μ F
	L_{ref}	Active inductor equivalent L_{ref}	2.5 mH

Figure 2 shows one of the implementations of variable active inductors studied in this paper [18]. It has the same functionality and position as the conventional magnetic inductor, which is connected in series with the DC link for grid-current sharpening and DC-link ripple mitigation. In contrast to the magnetic inductor, made of magnetic core and copper coil, it is made of the power electronic circuit including a high-frequency full-bridge bidirectional converter, a high-frequency filter, conditioning circuits, and a controller. By using the high-frequency circuit, it can reduce the size and weight. The full-bridge circuit is controlled as a variable impedance to emulate the performance of the magnetic inductor. Existing work only proves the basic concept of the active inductor. The practical reliability-oriented design of the active inductor and the variable inductance control will be studied in following section.

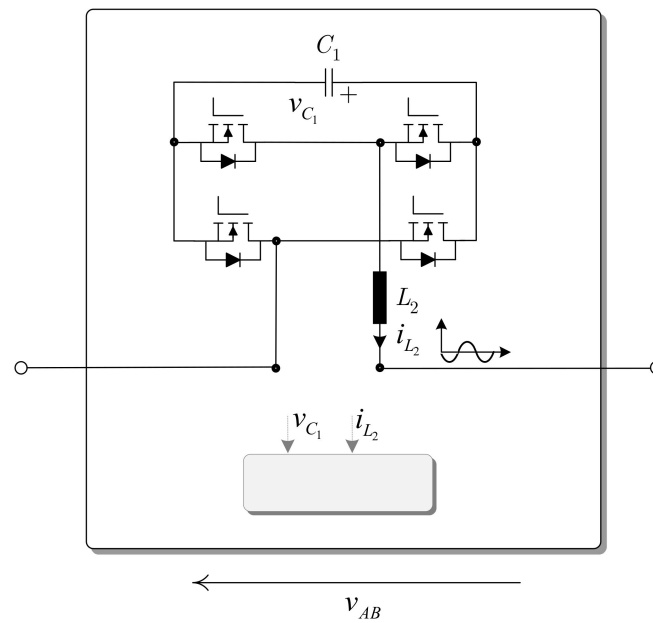


Figure 2. One implementation of the variable active inductor for the DC link of the motor-drive applications.

3. Reliability-Oriented Design of Variable Active Inductor

There are two reasons to study the reliability-oriented design of variable active inductors. First is the reliability requirement of the product. Magnetic inductors being reliable in power converters in common knowledge. In order to replace the magnetic inductor by using a variable active inductor, it is necessary to achieve the same level of reliability. The second reason is to identify the benefit of this technology from the practical of view. The comparison of the results of size, weight, and cost from magnetic inductors and active variable inductors should rely on the same reliability specifications. Then, the results would be meaningful. Based on the background, the flow chart based on reliability design is considered and shown in Figure 3.

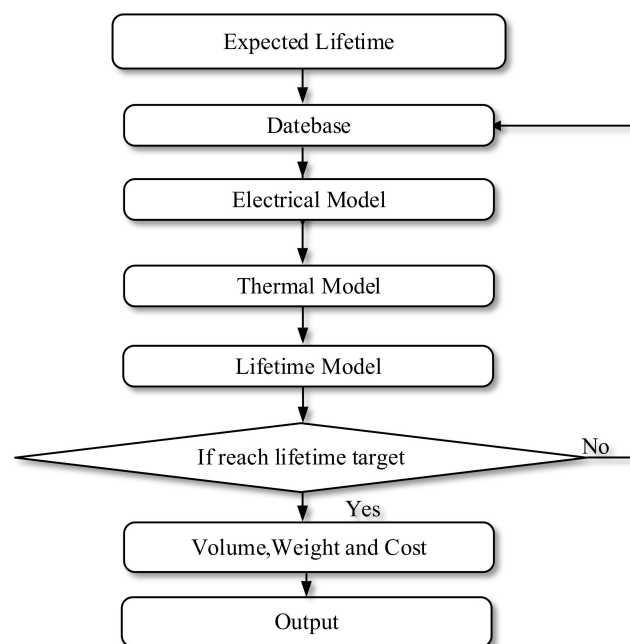


Figure 3. Flowchart of the reliability-oriented design procedure for the performance comparison of passive magnetic inductor and variable active inductor.

The reliability-oriented design flowchart includes eight steps [21,22]. The inputs of the design are the expected lifetime and operating conditions. Suitable devices are initially selected in the component database based on the operating conditions and expected lifetime. The database contains capacitors, inductors and switching devices. Then, the power losses of capacitors and switching devices are calculated by the electrical model. The power loss is used as an input to the thermal model, and the temperature of the capacitor and switching devices during operation is obtained by thermal stress analysis. Finally, the results of the thermal stress analysis are input to the lifetime model, and the lifetime of the capacitors and power semiconductors are estimated through the lifetime model. If the lifetime fulfills the expected requirements, the physical characteristics of the active inductor can be exported, otherwise, the devices continue to be reselected in the database until the expected lifetime is fulfilled [3].

3.1. Capacitor

3.1.1. Capacitor Selection

The voltage stress and current stress of the capacitor should be determined based on the operating conditions of the system before selecting the capacitor. For the active inductor module, the capacitor voltage to complete the DC-link capacitive energy conversion should satisfy as:

$$V_{dc} \geq |V_{ind}|$$

The current stress of the capacitor, by ignoring the power loss of the converter, can be calculated by the law of conservation of energy as:

$$I_c = \frac{V_{ind} I_{ind}}{V_{dc}}$$

where I_{ind} is the current flowing through the active inductor which can be calculated by the method in [23]. The final step in capacitor selection is to obtain the capacitance of the DC link from [23].

3.1.2. Electrical Model

The hotspot temperature of the capacitor changes with the power loss of the capacitor and affects the lifetime of the capacitor. Therefore, the power loss of capacitor is an important factor in determining its lifetime. The power loss of the capacitor can be calculated as [3]:

$$P_{loss} = \sum_{i=1}^n [ESR(f_i) \times I_{rms}^2(f_i)]$$

where $ESR(f_i)$ is the Equivalent Series Resistance (ESR) of the capacitor when the current frequency is f_i , and $I_{rms}(f_i)$ is the Root Mean Square (RMS) value of the harmonic current at the frequency f_i . The ESR of the capacitor and the RMS of the current can be derived from the electrical model.

3.1.3. Thermal Model

For electrolytic capacitors, the high temperature of the capacitor will accelerate the electrolyte vaporization and lead to the aging of the capacitor [3]. Based on the power loss of the capacitor derived in the previous step, the hotspot temperature of the capacitor can be calculated from the thermal model of the capacitor [3]:

$$T_h = T_a + R_{ha} P_{loss}$$

where T_a is the ambient temperature, R_{ha} is the thermal resistance of the capacitor hotspot to the environment.

3.1.4. Lifetime Model

For electrolytic capacitors, a generic lifetime model is as follows [3]:

$$L = L_0 \times \left(\frac{V}{V_0}\right)^{-n} \times 2^{\frac{T_0 - T_h}{10}}$$

where L and L_0 are the lifetime under operating and test conditions, respectively. V and V_0 are the voltages under operating and test conditions, respectively. T and T_0 are hotspot temperatures under operating and test conditions, respectively. The value of n for electrolytic capacitors usually varies from 3 to 5.

3.2. Power Semiconductors

3.2.1. Power Semiconductor Selection

The selection of the power semiconductor depends on its electrical stress and the required switching frequency of the system. The structure and principle of the active inductor circuit show that the voltage stress V_{sw} and current stress I_{sw} of the switching device are:

$$\begin{cases} V_{sw} = V_{dc} \\ I_{sw} = I_{ind} \end{cases}$$

3.2.2. Power-Loss Calculation

Power loss of power semiconductors mainly includes conduction loss and switching loss [24]:

$$P_{loss} = P_{CM} + P_{CD} + P_{swM} + P_{swD}$$

The conduction loss includes the conduction loss of the switching device P_{CM} and P_{CD} the equivalent diode [24]:

$$\begin{cases} P_{CM} = \frac{1}{T_{sw}} \int_0^{T_{sw}} (R_{DSon} \times i_D^2(t)) dt = R_{DSon} \times I_{Drms}^2 \\ P_{Cd} = \frac{1}{T_{sw}} \int_0^{T_{sw}} (u_{D0} \times i_F(t) + R_D \times i_F^2(t)) dt \\ = u_{D0} \times I_{Fav} + R_D \times I_{Frms}^2 \end{cases}$$

where I_{Drms} is equal to I_{indrms} , R_{DSon} is the on-resistance of the switching device, u_{D0} and R_D are the zero-current voltage of the diode on state and the diode on-state resistance, respectively. $i_D(t)$ and $i_F(t)$ are the transient currents flowing through the switch and diode, respectively. I_{Fav} is the average diode current and I_{Frms} is the root mean square diode current. The above parameters can be obtained from the data sheet of the switching device.

Power semiconductor switching loss consists of switching device loss and diode loss. The diode conduction loss can be ignored, and the switching loss is the product of switching energy and switching frequency:

$$\begin{cases} P_{swM} = (E_{onM} + E_{offM}) \times f_{sw} \\ P_{swM} = (E_{onD} + E_{offD}) \times f_{sw} \approx E_{onD} \times f_{sw} \end{cases}$$

where E_{onM} and E_{offM} are the turn-on energy loss and turn-off energy loss of the switching device, respectively, f_{sw} is the switching frequency and E_{onD} is the turn-on energy of the diode.

3.2.3. Thermal Model

The temperature variation of a power semiconductor is determined by the power loss and thermal resistance of the power semiconductor [24]:

$$\begin{cases} \Delta T = P_{loss} \times R_{th} \\ R_{th} = R_{jc} + R_{ch} + R_{ha} \end{cases}$$

where R_{jc} is the thermal resistance from the junction to the case, R_{ch} is the thermal resistance from the case to the heat sink, and R_{ha} is the thermal resistance of the heat sink to ambient.

3.2.4. Lifetime Model

The Bayerer model, which is a more comprehensive analytical model, is used for the prediction of power-switch lifetime. When using this model, it is important to specify the experimental conditions involved in the model before making lifetime predictions for the device [25]. The model equation is as follows:

$$N = A (\Delta T_j)^{-\beta_1} \exp\left(\frac{\beta_2}{T_{j,max} + 273}\right) t_{on}^{\beta_3}$$

where A , β_1 to β_3 are constants that can be proposed after data fitting, ΔT_j is the junction temperature variation of the power switch and $T_{j,max}$ is the maximum junction temperature of the power switch, t_{on} is the on-time of the power switch during the power cycle.

3.3. Inductor

The inductor has less degradation compared to power switches and capacitors, so the lifetime of the inductor is not considered in this paper. The selection of inductors is based on the Total Harmonic Distortion (THD) and ripple-current requirements of the inductor current. In addition, electrical stresses should be satisfied.

4. Variable Inductance Control for Performance Improvement

The control of the variable inductor includes two parts. The first part aims to generate the equivalent inductance reference based on the terminal information of the variable inductor. Another part is to realize this equivalent inductance reference by using closed-loop current control. The control diagram is shown in Figure 4. The parameter definitions are shown below.

V_{dc_ref} is the reference voltage of C_{dc} ,

V_{dc} is the actual voltage of the C_{dc} ,

R_{vir} is the virtual impedance of the active inductor,

I_{ind} is the current flowing through the active inductor,

I_{ind_ref} is the current reference value of the active inductor,

V_R is the virtual impedance voltage,

V_{ind} is the active inductor port voltage,

L_{ref} is the reference value of the equivalent inductance of the active inductance,

I_{ripple_ref} is the reference value of active inductor ripple current,

I_{ripple} is the actual ripple current of the active inductor.

In the equivalent inductance reference generation block, the input is the DC-link current limit and the measured DC-link current. By extracting the peak-to-peak current ripple and comparing it with the ripple limit, the control error can be obtained. Through a PI controller, the inductance reference can be derived. If the measured ripple is higher than the limit, the equivalent inductance value will increase to reduce the ripple, otherwise it will reduce to enlarge the ripple component.

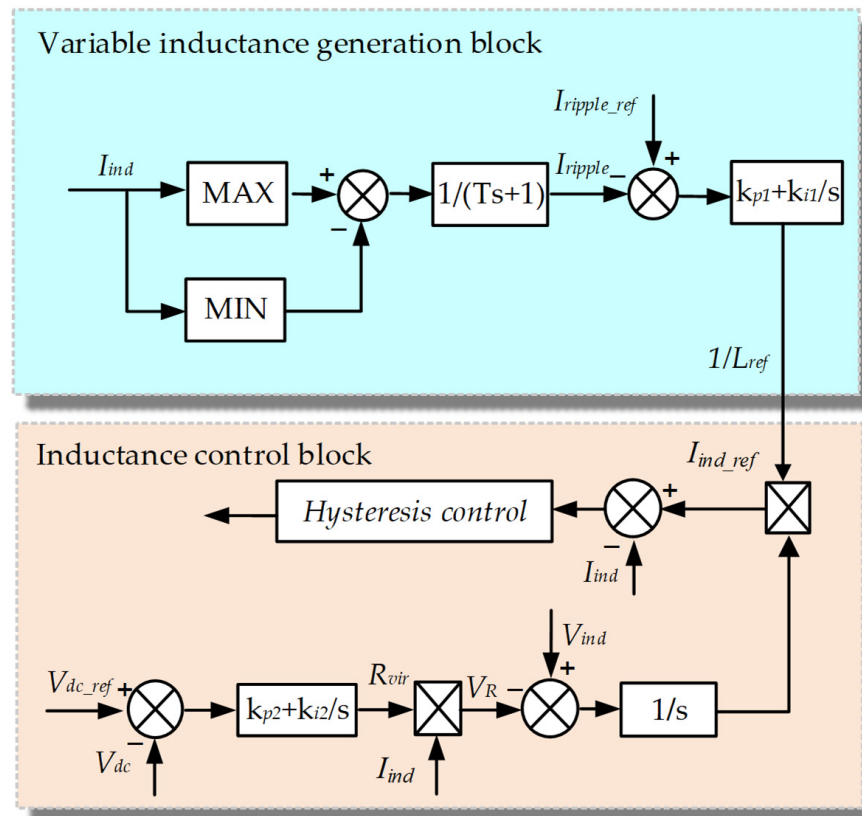


Figure 4. Control diagram of the variable active inductor.

In the inductance control block, there are two loops to achieve the certain inductance value and stabilize the variable inductor. The outer loop is the low-speed loop, used to stabilize the DC-link voltage inside of the active inductor. During operation, the active inductor will consume energy to support the power loss of the switches, filters, and other auxiliary components. The DC-link voltage inside of the active inductor could drop continually if there is no additional energy compensation. By using the voltage outer loop, the active power will be absorbed by the variable inductor to maintain the constant DC-link voltage. The input of the outer loop is the DC-link reference voltage and the measured voltage. Through a PI controller, the equated loss of a series' virtual resistance R_{vir} can be obtained. The product of the virtual resistance and the inductor current is the voltage drop of the virtual resistance, V_R . This result is subtracted from the port voltage, V_{ind} , to be the actual voltage drop of the inductor. The voltage of the inductor obtained through the voltage loop is used as the input to the current loop. The function of the current loop is to track the reference current calculated from the equivalent inductance reference. The current loop controls the current of the active inductor according to following equation.

$$I_{ind_ref} = \frac{1}{L_{ref}} \int (V_{ind} - V_r) dt$$

The resulting current error signal is fed to the hysteresis controller to generate the drive signals for the power switches that control the operation of the H-bridge, and the terminal impedance is controlled as a magnetic inductor by the current loop.

Simulation results of an ASD system with a magnetic inductor and variable active inductor are provided for comparison to support the theoretical analysis in Figure 5. In the ASD system with the passive magnetic inductor, when the grid voltage is balanced, the grid-side current is a continuous current. There are 6-times the fundamental current at the DC link and the load side, as shown in the red curve. In the system when the

active inductor replaces the passive inductor, it can be seen that the waveforms are totally overlapped, which means the active variable inductor can achieve the same performance as the passive magnetic inductor in this ASD system. It proves the functionality of the fixed-inductance control method.

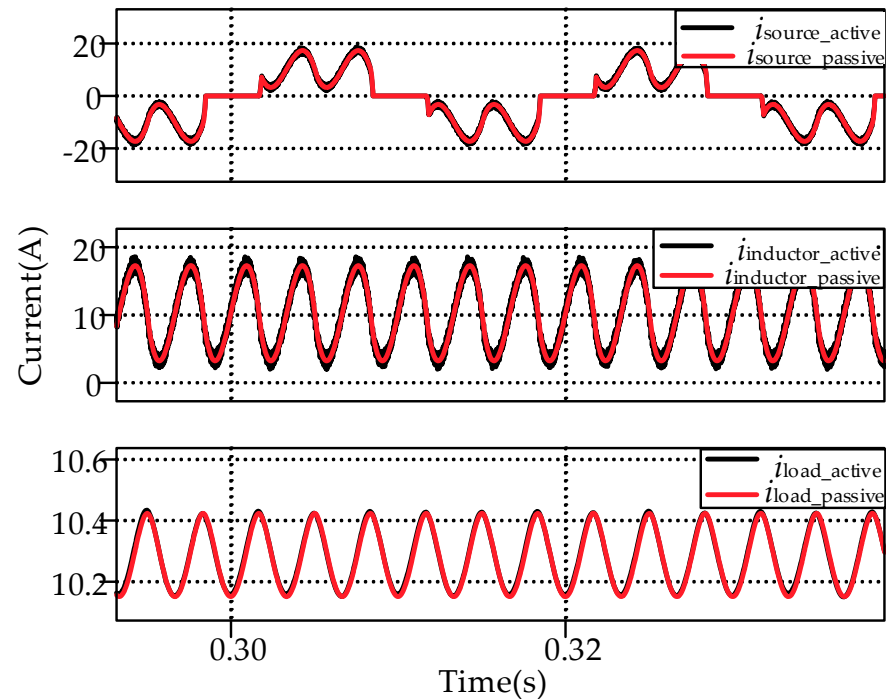


Figure 5. Simulation results comparison between passive magnetic inductor and active variable inductor under balanced grid voltage condition. Top: grid-side current; Middle: DC-link current; Bottom: load current.

The simulation results prove the variable inductance control as shown in Figure 6. The test condition is 3% unbalanced grid-voltage amplitude. When the grid voltage becomes unbalanced, the three-phase diode bridge rectifier will be forced into the single-phase operation mode. There it will introduce two times the fundamental frequency oscillation at the DC link beside six times the fundamental oscillation. The cut-off frequency of the low-pass filter is 10 Hz. Kp1 and Ki1 are 1 and 150, respectively. Kp2 and Ki2 are 0.03 and 0.5, respectively. The bandwidth of the hysteresis controller is 0.5 A. By using the existing magnetic inductor, the filter characteristic is constantly fixed, therefore, the oscillations at the grid unbalances are severe. However, when the ASD system is implemented with the variable active inductor, the equivalent inductance is adaptively increased from 2.5 mH to 8 mH with the DC-link oscillation, instead of fixed filtering characteristics. From the simulation, it can be seen that the DC-link ripple and the load-current ripple can be reduced significantly, due to the equivalent inductance of the variable active inductor being updated automatically from 2.5 mH to 8 mH. As a comparison, the DC-link ripple of the magnetic inductor is much higher than the expected, which raises the stress of the inverter stage and could lead to higher failure rate and shorter lifetime.

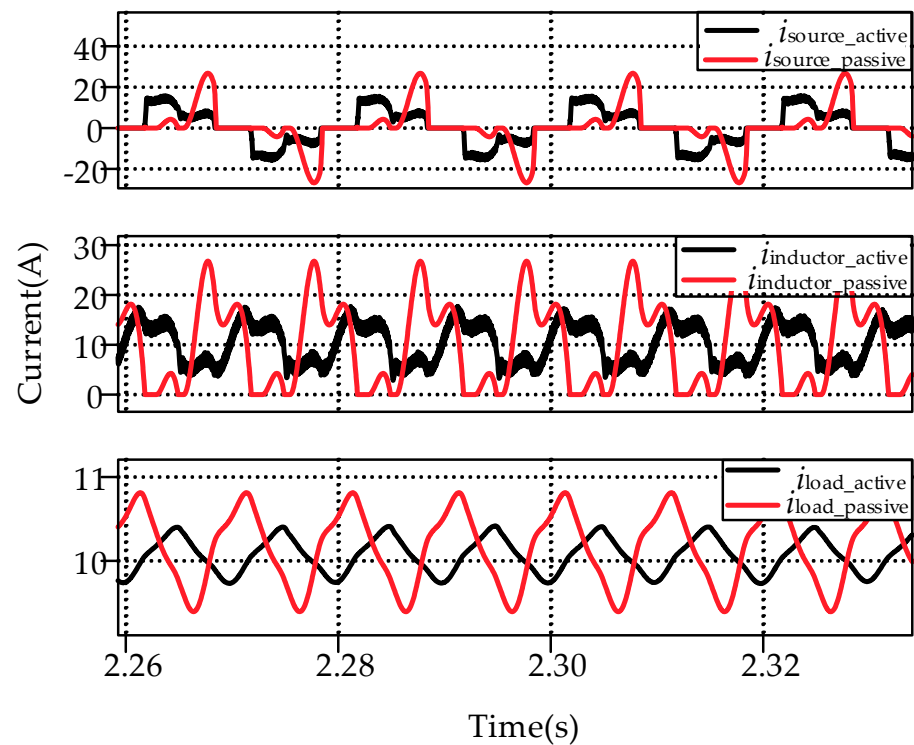


Figure 6. Simulation results comparison between passive magnetic inductor and active variable inductor under unbalanced grid voltage condition. Top: grid-side current; Middle: DC-link current; Bottom: load current. Red: passive magnetic inductor; Black: variable active inductor.

5. Experimental Verification of the Variable Inductor

A prototype is built in the lab to prove the physical characteristics of the variable active inductor, which is shown in Figure 7. It is designed for the DC link of a 7.5 kW ASD system. In order to emulate the operating condition of the ASD system, an equivalent testing system is built in the lab. The first stage uses a programmable voltage source to emulate the grid voltage, and then is connected with a front-end diode bridge rectifier. The load inverter is simplified by using a resistor load. Unbalanced grid voltage at 3% amplitude at one phase is considered to emulate the unbalanced grid-voltage case. Even though the harmonics content is different from the real case, the low-frequency six times and two times the fundamental frequency harmonics are the same with the field applications. Therefore, it has no effect on the accuracy of the experimental verification. The prototype built in the lab is shown below. There are two PCBs assembled together, where one board is the power stage and another one is the conditioning and controller circuit. Separate design could reduce the noise transmission from the power stage to the signal stage. From the pictures of the prototypes, it can be seen that the variable active inductor has a smaller size, lighter weight, and lower height compared with the passive magnetic inductor. The estimated power loss of the device, capacitor, and filter inductor are 2.5 W, 1.8 W and 10 W, respectively. The control frequency of the prototype is 20 kHz to track the harmonics at six times and two times fundamental frequency. The control parameters are shown below. The detailed comparison and the verification of the control methods are discussed below.

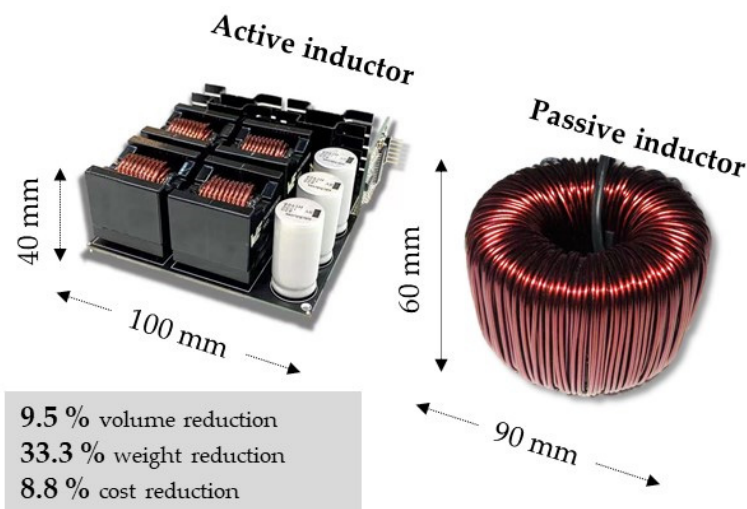


Figure 7. Comparison of the variable active inductor prototype and the passive magnetic inductor prototype built in lab.

5.1. Physical Characteristics Comparison between Magnetic and Active Inductor

The physical characteristics are compared between magnetic and active inductor, with results shown in Table 2. The active inductor component selection is based on the reliability-oriented component sizing procedure, where the designed lifetime is 10 years. For the passive magnetic inductor, it is commonly assumed that it is much reliable compared with the components in the power converter, so the reliability is sufficient. In this case, the physical characteristics can be benchmarked, and the results are shown in Figure 8. It can be seen that all the physical characteristics can be optimized by using a variable active inductor, especially the weight of the active inductor. By using the semiconductor circuit, the weight is much lower than the magnetic-core- and copper-coil-based inductor, which is a great contribution to weight-sensitive applications, such as EV, traction, aircraft and so on.

Table 2. Reliability-oriented component sizing results.

		Value	Product number	Volume(L)	Weight(kg)	Cost(EUR)
Passive inductor	L_{ref}	2.5 mH/17 A	Customized	0.486	0.9	52.5
	Total value	-	-	0.486	0.9	52.5
Active inductor	L_{filter}	65 μ H/17 A	WurthElektronik 7443783533650	0.174	0.4	34
	C_{dc}	820 μ F/100 V	Nichicon UBY2A821MHL	0.023	<0.01	3.4
	Mosfet	43 A/100 V	Infineon IPP180N10N3GXKSA1	0.003	<0.01	1.8
	Heatsink	-	Aavid 507222	0.063	<0.01	1.2
	Driver	-	Infineon IRS2007SPBF	-	<0.01	0.7
	Controller	-	Microchip dsPIC33F	-	<0.01	1.8
	Others	-	-	0.177	0.2	5
	Total value	-	-	0.44	0.6	47.9

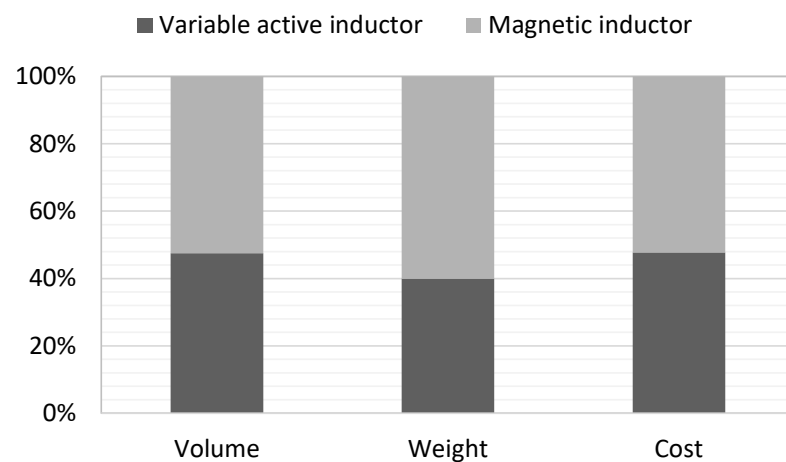


Figure 8. Physical characteristics comparisons between variable active inductor and magnetic inductor. Dark grey: variable active inductor; Grey: Magnetic inductor.

5.2. Verification of the Electrical Characteristics of the Variable Inductor under Balanced Grid Condition

The first step to prove the effectiveness of the active variable inductor is to compare the electrical performance with the magnetic inductor with the same inductance value. Due to the power limit in the lab, downscale testing is conducted, where the experimental results of the ASD with the active inductor is shown in Figure 9. It can be seen that when the grid voltage is balanced, there will be six times the fundamental frequency at the DC link. From the comparison in (a–d), it can be seen that the variable active inductor can achieve the same performance as the passive magnetic inductor. Therefore, it can work well and replace it for the normal operation.

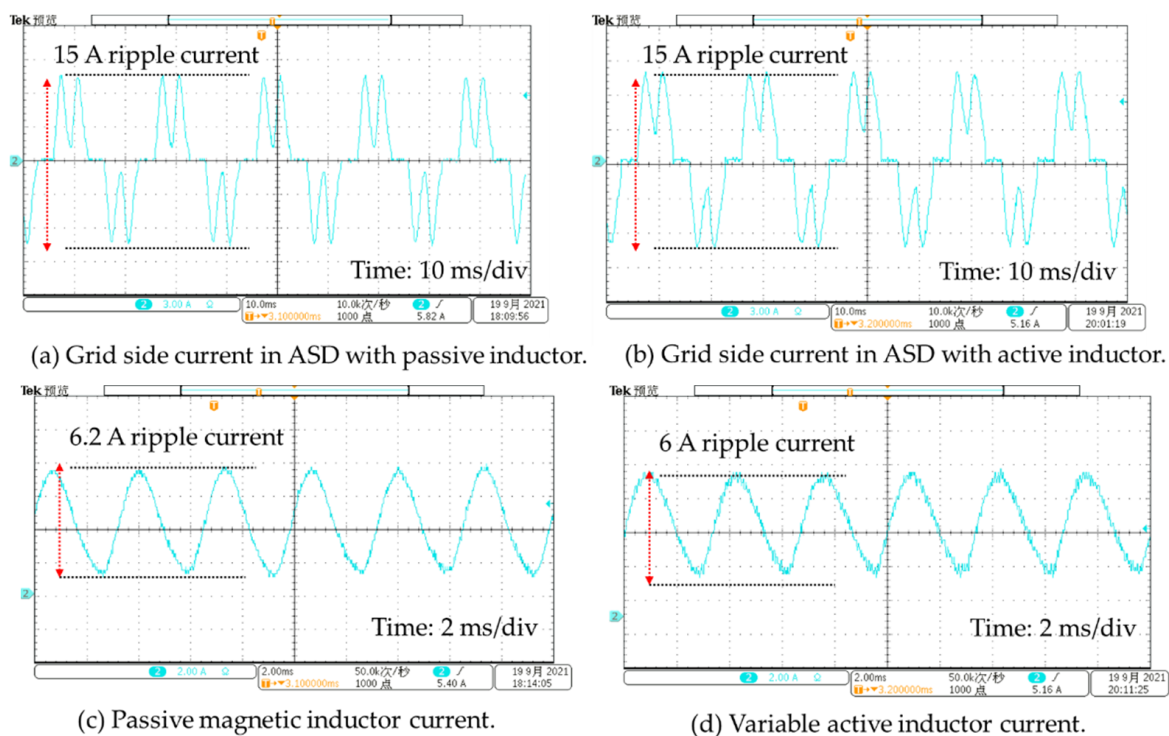


Figure 9. Test results of the passive magnetic inductor and variable active inductor under the unbalanced grid voltage condition in ASD system. (a) Grid side current in ASD with passive inductor; (b) Grid side current in ASD with active inductor; (c) Passive magnetic inductor current; (d) Variable active inductor current.

5.3. Verification of Electrical Characteristics of the Variable Inductor under Unbalanced Grid Condition

In real applications, the unbalanced grid voltage will introduce two times the fundamental harmonics at the DC link. The existing fixed inductor cannot filter out these harmonics, leading to high oscillation. The proposed variable active inductor can adaptively change the inductance value to mitigate the high ripple. Experimental testing to prove the effectiveness of the variable active inductor in the unbalanced grid voltage conditions are shown in Figure 10. It can be seen that when the grid voltage is unbalanced, the grid-side current will distort and the DC-link current will have a higher ripple, which includes both six times the fundamental harmonics and the two times the fundamental harmonics. By using the active variable inductor, the harmonics at the DC link can be reduced to 60% of the ripple in the passive inductor case study. This will be helpful to reduce the stress and enhance the stability of the motor-drive system.

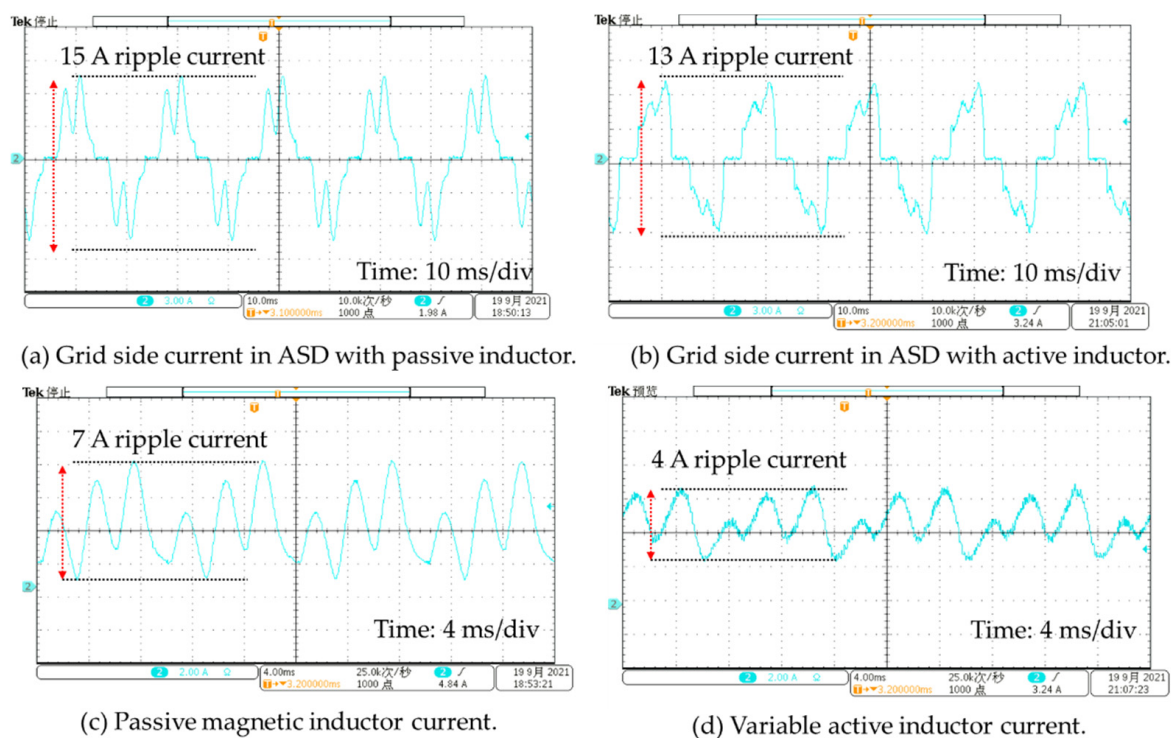


Figure 10. Test results of the passive magnetic inductor and variable active inductor under the unbalanced grid voltage condition in the ASD system. (a) Grid side current in ASD with passive inductor; (b) Grid side current in ASD with active inductor; (c) Passive magnetic inductor current; (d) Variable active inductor current.

6. Discussion and Future Perspectives

This paper studies the benefits of the active inductor compared with the conventional magnetic inductor from the practical point of view and proposes a novel variable active inductor for the performance improvement of motor drive, considering real grid conditions. Even though it has been fully discussed and the concept has been proven, there are still some interesting aspects to be studied in the future:

- The benefits of the active inductor at a range of power rating applications are different. It is necessary to model the performance in a wide range and identify the best region for use.
- The applications of variable inductor are not limited to the DC link. It can also be used as the fixed AC magnetic inductor and variable AC inductor. The corresponding circuit structure and control are necessary to be studied in the future.

- The plug-and-play functionality is preferred due to the conventional magnetic inductor being a two-terminal component, which is easy to use. Practical design and implementation are interesting to study.

There are also application limits to the variable inductor. For high-frequency harmonics applications, such as kHz and MHz, ultrahigh-frequency switching devices are needed to implement the variable active inductor. The benefit of the variable inductor is not clear. The physical characteristics and cost could limit the application of the variable inductor, which requires further study.

7. Conclusions

This paper proposes a novel variable inductor for the DC link of an ASD system. It can adaptively change the inductance under different conditions and effectively improve the electrical and physical characteristics in principle. The reliability-oriented design is first studied to demonstrate the benefits of the variable active inductor. All the components are based on the same design procedures and same reliability targets, so that the comparison between solutions is more useful. It considers the practical factors (e.g., size, weight, cost, and reliability) compared to the proof-of-concept studied in previous work. A novel variable inductance control method is proposed to stabilize the system under normal and abnormal operating conditions. The key conclusions are summarized below:

- Based on the reliability-oriented design, the physical characteristics in terms of size, weight, and cost of the variable inductor for the commercial products can be reduced to maximum of 30%;
- By online adaptive tuning the inductance value, the oscillation at the DC link can be mitigated at both the unbalanced and balanced grid voltage conditions.

Author Contributions: Conceptualization, Q.W. and B.L.; methodology, Z.K. and F.L.; validation, Z.K., and F.L.; investigation, Z.K., J.W.; data curation, Z.K., J.W.; writing—original draft preparation, Q.W. and Z.K.; writing—review and editing, Q.W. and B.L.; supervision, Q.W. and B.L. All authors have read and agreed to the published version of the manuscript.

Funding: This work was supported by project of National Natural Science Foundation of China (Grant No: 51777146, 51977163).

Data Availability Statement: Data available in a publicly accessible repository.

Conflicts of Interest: The authors declare no conflict of interest.

References

1. Zare, F.; Soltani, H.; Kumar, D.; Davari, P.; Delpino, H.A.M.; Blaabjerg, F. Harmonic emissions of three-phase diode rectifiers in distribution networks. *IEEE Access* **2017**, *5*, 2819–2833. [\[CrossRef\]](#)
2. Hinkkanen, M.; Luomi, J. Induction motor drives equipped with diode rectifier and small dc-link capacitance. *IEEE Trans. Ind. Electron.* **2008**, *55*, 312–320. [\[CrossRef\]](#)
3. Wang, H.; Blaabjerg, F. Reliability of Capacitors for DC-Link Applications in Power Electronic Converters—An Overview. *IEEE Trans. Ind. Appl.* **2014**, *50*, 3569–3578. [\[CrossRef\]](#)
4. Wen, H.; Xiao, W.; Wen, X.; Armstrong, P. Analysis and Evaluation of DC-Link Capacitors for High-Power-Density Electric Vehicle Drive Systems. *IEEE Trans. Veh. Technol.* **2012**, *61*, 2950–2964. [\[CrossRef\]](#)
5. Rajashekara, K.S.; Rajagopalan, V.; Sevigny, A.; Vithayathil, J. DC Link Filter Design Considerations in Three-Phase Voltage Source Inverter-Fed Induction Motor Drive System. *IEEE Trans. Ind. Appl.* **1987**, *IA-23*, 673–680. [\[CrossRef\]](#)
6. Dzhankhotov, V.; Pyrhönen, J. Passive LC Filter Design Considerations for Motor Applications. *IEEE Trans. Ind. Electron.* **2013**, *60*, 4253–4259. [\[CrossRef\]](#)
7. Council of European Energy Regulators (CEER). *5th Ceer Benchmarking Report on the Quality of Electricity Supply*; Council of European Energy Regulators (CEER): Brussels, Belgium, 2011.
8. Kolar, J.W.; Friedli, T. The Essence of Three-Phase PFC Rectifier Systems—Part I. *IEEE Trans. Power Electron.* **2013**, *28*, 176–198. [\[CrossRef\]](#)
9. Wang, H.; Davari, P.; Wang, H.; Kumar, D. Lifetime estimation of DC-Link capacitors in adjustable speed drives under grid voltage unbalances. *IEEE Trans. Power Electron.* **2019**, *34*, 4064–4078. [\[CrossRef\]](#)
10. Von Jouanne, A.; Banerjee, B. Assessment of voltage unbalance. *IEEE Trans. Power Deliv.* **2001**, *16*, 782–790. [\[CrossRef\]](#)

11. Wang, H.; Liserre, M.; Blaabjerg, F. Toward reliable power electronics: Challenges, design tools, and opportunities. *IEEE Ind. Electron. Magazine* **2013**, *7*, 17–26. [[CrossRef](#)]
12. ANSI C84.1. *American National Standard for Electric Power Systems and Equipment-Voltage Ratings (60 Hertz)*; NEMA: Rosslyn, VA, USA, 2006.
13. Lee, K.; Jahns, T.; Venkataramanan, G.; Berkopec, W. DC bus electrolytic capacitor stress in adjustable-speed drives under input voltage unbalance and sag conditions. In Proceedings of the Conference Record of the 2004 IEEE Industry Applications Conference, 2004. 39th IAS Annual Meeting, Seattle, WA, USA, 3–7 October 2004. [[CrossRef](#)]
14. Wang, H.; Wang, H. Capacitive dc links in power electronic systems reliability and circuit design. *Chin. J. Elect. Eng.* **2018**, *4*, 29–36.
15. Wang, H.; Wang, H.; Zhu, G.; Blaabjerg, F. An overview of capacitive dc links—Topology derivation and scalability analysis. *IEEE Trans. Power Electron.* **2020**, *35*, 1805–1829. [[CrossRef](#)]
16. Wang, H.; Wang, H. A two-terminal active capacitor. *IEEE Trans. Power Electron.* **2017**, *32*, 5893–5896. [[CrossRef](#)]
17. Funato, H.; Kawamura, A. Proposal of variable active-passive reactance. In Proceedings of the 1992 International Conference on Industrial Electronics, Control, Instrumentation, and Automation, San Diego, CA, USA, 13–13 November 1992; Institute of Electrical and Electronics Engineers (IEEE): Piscataway, NJ, USA, 2003; pp. 381–388.
18. Rana, D.; Hafez, B.; Garg, P.; Essakiappan, S.; Enjeti, P. Analysis and design of active inductor as DC-link reactor for lightweight adjustable speed drive systems. In Proceedings of the 2014 IEEE Energy Conversion Congress and Exposition (ECCE), Pittsburgh, PA, USA, 14–18 September 2014; Institute of Electrical and Electronics Engineers (IEEE): Piscataway, NJ, USA, 2014; pp. 3243–3250.
19. Dai, W.; Enjeti, P.; Qiu, D. Advanced active output filter for low acoustic noise adjustable speed drive (ASD) system. In Proceedings of the 2016 IEEE International Power Electronics and Motion Control Conference (IPEMC-ECCE Asia), Hefei, China, 22–26 May 2016; pp. 3646–3653.
20. Das, J. Passive filters—potentialities and limitations. *IEEE Trans. Ind. Appl.* **2003**, *40*, 232–241. [[CrossRef](#)]
21. Wang, H.; Wang, H. Performance evaluation of a two-terminal active Inductor in the DC-link filter of a three-phase di-ode bridge rectifier. In Proceedings of the IEEE APEC, Anaheim, CA, USA, 17–21 March 2019; pp. 2844–2848.
22. Wang, H.; Wang, H. A Two-Terminal Active Inductor with Minimum Apparent Power for the Auxiliary Circuit. *IEEE Trans. Power Electron.* **2019**, *34*, 1013–1016. [[CrossRef](#)]
23. Sakui, M.; Fujita, H.; Shioya, M. A method for calculating harmonic currents of a three-phase bridge uncontrolled rectifier with DC filter. *IEEE Trans. Ind. Electron.* **1989**, *36*, 434–440. [[CrossRef](#)]
24. Graovac, D.; Pürschel, M.; Kiep, A. MOSFET Power Losses Calculation Using the DataSheet Parameters. Infineon Technologies AG. Available online: www.infineon.com (accessed on 31 July 2006.).
25. Bayerer, R.; Herrmann, T.; Licht, T.; Lutz, J.; Feller, M. Model for Power Cycling lifetime of IGBT Modules - various factors influencing lifetime. In Proceedings of the 2008 International Conference on Integrated Power Electronics Systems, Nuremberg, Germany, 11–13 March 2008; pp. 1–6.